Materials Today Bio 36 (2026) 102742

Contents lists available at ScienceDirect

Materials Today Bio

journal homepage: www.journals.elsevier.com/materials-today-bio

Microfluidic 3D-printed MSC-laden bioactive hydrogel for intrauterine adhesion prevention and endometrial regeneration

Yizuo Song [a,1], Rong Ma [a,1], Baozhu Yi [a], Qingfeng Zhou [a], Xiaosheng Li [a], Yujia Zhou [a], Ying Hua [a], Luoran Shang [a,b,*], Xueqiong Zhu [a,**]

[a] Department of Obstetrics and Gynecology, The Second Affiliated Hospital of Wenzhou Medical University, Wenzhou, 325027, Zhejiang, China
[b] Zhongshan-Xuhui Hospital, The Shanghai Key Laboratory of Medical Epigenetics, Institutes of Biomedical Sciences, Fudan University, Shanghai, 200032, China

ARTICLE INFO

Keywords:
Mesenchymal stem cells
3D bioprinting
Hydrogel scaffold
Intrauterine adhesion
Endometrium regeneration

ABSTRACT

Increasing occurrence of intrauterine adhesion (IUA) is a serious threat to the reproductive health of women in recent years. However, treatment options remain limited. Mesenchymal stem cell (MSC)-based therapies have shown a promising regenerative capacity of injured endometrium but have limited effectiveness by the low survival duration of transplanted cells. Herein, we present a bioactive hydrogel scaffold loaded with adipose tissue-derived MSC (AT-MSC) by using a three-dimensional (3D) bioprinting technology, which combines the characteristics of the synthetic thermos-responsive material PF-127 and the natural-derived, photo-polymerizable material GelMA. The composite hydrogel scaffold shows enhanced mechanical as well as biocompatibility. In addition, the porous structure endows the 3D-printed scaffold with a favorable growing environment for MSC and increase the retention rate of cells. Finally, the dual repair effects of the MSC-laden gel scaffold on endometrial damage and regeneration are validated in a rat IUA model. This study demonstrates that the composite system could improve neovascularization, increase number of glands, and ameliorate fibrotic formation of endometrium. Thus, it is believed that such bioactive MSC-loaded scaffold is a promising candidate for prevention of IUA with reliable endometrial regeneration properties.

1. Introduction

Intrauterine adhesion (IUA) is characterized as the scar tissue formation in the uterine cavity after endometrial damage, which is also called Asherman syndrome. Severe IUA can cause infertility in women within reproductive age [1]. Therefore, it is vital to rebuild the uterine cavity and repair the injured endometrium for IUA treatment. Currently, the most common treatment for IUA is hysteroscopic transcervical resection of adhesion (TCRA), followed by using physical barriers for preventing re-adhesion after surgery and hormone therapy for endometrial regeneration [2]. However, postoperative adhesions and low clinical pregnancy rates continue to be problems for patients with severe IUA [3,4]. Cellular therapeutics such as mesenchymal stem cell (MSC) have been employed as an alternative strategy, which exerts powerful regenerative and inflammatory regulation abilities [5]. Recently, MSC-based therapies have emerged as new and potential options for tissue regeneration [6,7]. Indeed, MSCs have been shown to be capable of repairing damaged tissues and restoring endometrial structure and function [8,9]. However, the therapeutic efficacy of MSCs remains hampered by limitations in existing delivery systems, such as short cell retention time and low survival rates post-transplantation [10]. These challenges are particularly evident when compared to recent advances in biomaterial-assisted MSC delivery, including the use of various hydrogels such as hyaluronic acid and innovative three-dimensional (3D) printing strategies [11,12]. Therefore, it is paramount to developing novel strategies to efficiently deliver MSC and promote endometrial repair.

3D bioactive hydrogels have been increasingly used as scaffold materials for cell encapsulation or drug delivery in the recent past [5,11,13–15]. In the current study, we propose an MSC-loaded bioactive

* Corresponding author. Zhongshan-Xuhui Hospital The Shanghai Key Laboratory of Medical Epigenetics Institutes of Biomedical Sciences Fudan University Shanghai, 200032, China.
** Corresponding author. Department of Obstetrics and Gynecology The Second Affiliated Hospital of Wenzhou Medical University No.109 Xueyuan Xi Road, Wenzhou, 325027, China.
E-mail addresses: luoranshang@fudan.edu.cn (L. Shang), zjwzzxq@163.com (X. Zhu).
[1] **Note:** Song Y and Ma R contributed equally to this work.

https://doi.org/10.1016/j.mtbio.2025.102742
Received 14 June 2025; Received in revised form 23 November 2025; Accepted 23 December 2025
Available online 27 December 2025

hydrogel scaffold with customizable shapes for repairing injured endometrium, as illustrated in Fig. 1. For the treatment of IUA, MSCs can be embedded into the bioactive hydrogel to exert curative effects on endometrial regeneration. However, conventional scaffolds still fall short of providing optimal bioactive abilities [12]. Pluronic F-127 (PF-127) is a synthetic compound and has been approved by the Food and Drug Administration (FDA). PF-127 has several therapeutic advantages, such as low toxicity, good biocompatibility, and thermo-reversibility [16]. A moderately concentrated solution of PF-127 in aqueous media is liquid at room temperature, but can be solidified at physiological temperatures [17,18]. Gelatin methacryloyl (GelMA), a photocrosslinkable gelatin derivative, provides natural cell-adhesive motifs, supports cell viability, and allows structural stabilization via ultraviolet (UV) crosslinking. The combination of PF-127 and GelMA thus enables both printability and bioactivity, making it suitable for MSC delivery and endometrial regeneration. Conventional 3D printing approaches, particularly those based on extrusion-based methods, are often limited by low resolution, poor stability, and restricted functionality [19]. Microfluidics, defined as the technology for precise manipulation of fluids within microscale channel networks through modulation of fluid composition and flow rates, offers a promising alternative [20–24]. The integration of 3D printing with microfluidic platforms allows accurate regulation of fluid behavior in microchannels, demonstrating significant potential for fabricating high-precision, multi-component, and multifunctional bio-scaffolds [25].

Herein, we prepare the bioactive scaffolds using a microfluidic-assisted 3D printing method for delivering MSC and regenerating endometrium. Utilizing the microfluidic 3D printing technique [25,26], hydrogel fibers in micron-scale composed of GelMA and PF-127 were produced and subsequently assembled into 3D structures through a sequential layering process. The composite scaffold was exposed to UV light to achieving the crosslinking polymerization of GelMA components, and the strength of the hydrogel was further improved owing to the PF-127 component inside the hydrogel scaffolds. With this, the GelMA component in the fabricated scaffolds contribute to maintaining the viability of MSC within the hydrogel structures. We demonstrate that the GelMA/PF-127 (G/P) composite scaffolds loaded with MSC (MSC@G/P) could greatly promote endometrial repair by reducing inflammation, promoting cell growth, and boosting neovascularization. Consequently, the bioactive scaffolds created by 3D printing hold great potential for MSC delivery and endometrial regeneration.

2. Experimental section

2.1. Materials

GelMA and PF-127 were purchased from Sigma-Aldrich (USA). Lithium phenyl(2,4,6-trimethyl benzoyl) phosphinate (LAP) was supplied by Macklin (Shanghai, China). Penicillin-streptomycin (Pen-Strep) solution, Calcein-AM and Cell Counting Kit-8 (CCK-8) assay and the reactive oxygen species (ROS) assay kits were purchased from Beyotime (Shanghai, China). Pregnant mere serum gonadotropin (PMSG), and kits for hematoxylin and eosin staining (H&E) and Masson's Trichrome staining were obtained from Solarbio (Beijing, China). Antibodies against Ki-67, alpha-smooth muscle actin (α-SMA) and estrogen receptor alpha (ESRα), all produced from rabbits, were bought from Abcam (USA). The rabbit anti-mouse CD31 antibody was provided by Servicebio (China). Proteintech (Chicago, USA) supplied the rabbit anti-mouse tumor necrosis factor-alpha (TNF-α) and leukemia inhibitory factor (LIF) antibodies. From Solarbio (Beijing, China), goat anti-mouse IgG-FITC and goat anti-rabbit IgG-Cy3 were purchased. Human umbilical vein endothelial cells (HUVECs) were purchased from ScienCell (USA).

2.2. MSCs culture and characterization

The experiments involving human tissues were approved by the Ethical Committee of the Second Affiliated Hospital of Wenzhou Medical University (YS2024-026). Human adipose tissues were collected from three full-term healthy pregnant women (aged 23–30 years) with the written informed consent, who underwent cesarean section in the Second Affiliated Hospital of Wenzhou Medical University. The human adipose tissue-derived MSC (AT-MSC) used in the current study was

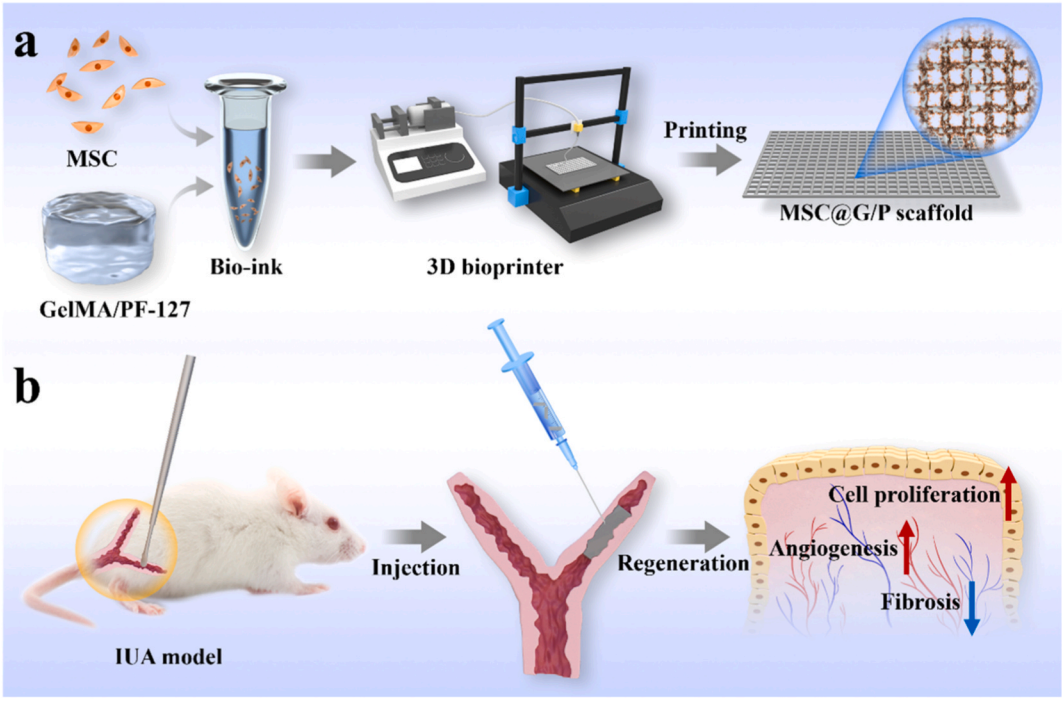

Fig. 1. Schematic illustration of the bioactive 3D-printed hydrogel scaffolds for MSC delivery and endometrial regeneration. (a) MSC was incorporated into scaffolds created using 3D printing technology. (b) MSC-laden scaffolds were administrated into the injured endometrium of rats with IUA to promote endometrial regeneration.

acquired and expanded according to our previous study [27]. In brief, the adipose samples were washed with PBS to remove any blood clots and cut into 1 mm^3 of small pieces. Then, the fragmented tissue masses were digested by mixing with 0.75 mg/ml Collagenase I and incubated at 37 °C for 1 h, with manual mixing every 15 min. After neutralization by the complete medium, the digested cell clusters were filtered via a 100-μm nylon mesh and the cell debris were removed. The obtained cells were centrifugated at 1200 rpm for 10 min. The MSC was seeded and grown in low-glucose Dulbecco's Modified Eagle's Medium (DMEM) supplemented with 10 % fetal bovine serum (FBS) and 1 % Pen-Strep, and maintained at a 37 °C in a humidified incubator with 5 % CO_2. Cell passage was performed when 80 % confluence was reached. MSCs between passages 3–6 (P3-P6) were used for the following experiments.

The expanded AT-MSC was identified by flow cytometric analysis and *in-vitro* differentiation assay. For flow cytometric analysis, AT-MSC was harvested, centrifuged, and incubated with a panel of antibodies in dark for 30 min. Subsequently, the immunophenotype of MSC was analyzed by the flow cytometer (Beckman, USA). For *in-vitro* differentiation assay, MSC was seeded on a 24-well plate at a density of 5×10^3 per well. After cells reaching 70 % confluence, the specific media for adipogenesis or osteogenesis were added into the matched well and changed every 3 days. After 3 weeks of incubation, the differentiated cells were fixed and stained by Oil Red O or Alizarin Red S solutions. Finally, the stained cells were observed under the microscope.

2.3. Microfludic printing of GelMA/PF-127 scaffolds

GelMA pre-gel of 15 % (w/v) (with 0.1 % LAP) was combined with 15 % (w/v) PF-127 solution to create bioink for microfluidic printing of G/P scaffolds. Printing was performed using a coaxial microfluidic printhead equipped with copper-made nozzle and featuring an inner channel diameter of 0.8 mm and an outer channel diameter of 0.9 mm. The prepared bioink was transfused into a 5-ml syringe, which was then mounted on a microfluidic pump. All printing procedures were performed at 22 °C. Throughout the process, the flow rate of bioink was set at 3 ml/h, while the printhead moved at a speed of 5 mm/s along a pre-programmed path, with a layer height of 200 μm and an inter-filament spacing of 250 μm. The deposited structures of scaffold were immediately crosslinked under UV light at 60 % of the maximum power density during printing process. The structures of scaffold were further strengthened by 100 % power density UV exposure after primary printing. All components utilized in scaffold preparation were sterilized overnight using UV light for cellular and animal experiments.

2.4. Characterization of GelMA/PF-127 scaffolds

A freeze-drying procedure followed by gold sputtering was performed on the G/P scaffold before imaging. Images of the scaffolds' porous structure were obtained using a scanning electron microscope (SEM; FE-SEM, SU8010, Hitachi, Japan). Then, the compression test was performed using a universal testing machine (Instron 5944, USA). A discovery hybrid rheometer-2 (DHR-2) (TA Instruments, USA) was then employed to measure the hydrogels' rheological behavior.

2.5. Biocompatibility of GelMA/PF-127 scaffolds

The MSC and scaffolds were co-cultured in 24-well plates for 1, 3 and 5 days. Then, CCK-8 working solution (500 μl) was introduced into each well for further incubation for 2 h at 37 °C. A microplate reader (Bio-Tek, USA) was used to determine the absorbance at 450 nm.

Subsequently, the viability of MSC cultured within the G/P scaffold was assessed through live cell staining with Calcein-AM. A Nikon inverted fluorescence microscope (Japan) was used to observe the live cells after 1, 3 and 5 days of culture.

2.6. In vitro endometrial regeneration ability of bioactive scaffolds

First, the conditional medium (CM) was prepared by co-culturing different scaffolds with MSCs using 0.5-μm pore size transwell filters (Corning, USA). A total of 3×10^4 MSCs were grown for 1, 3, and 5 days, respectively, based on each experimental group. After centrifugation for 5 min at 1000 rpm, the supernatant media were passed through a filter with a 0.22-μm diameter (Corning, USA).

For proliferation experiment, we placed HUVECs (1×10^4 cells per well) in the bottom chamber of 24-well plate, and we added 100 μl of CM in the top chamber of a filter with 8-μm pores (Corning, USA). The optical density (OD) value was measured using a microplate reader on days 1, 3 and 5.

For migration assay, HUVECs (1×10^4 cells per well) were loaded on the upper chamber of 24-well plate, and the lower chamber was filled with 500 μl of CM. HUVECs were stained with crystal violet (0.5 %) after 24-h of co-culture and observed. In tube formation test, HUVECs were seeded in 48-well plates on Matrigel with 5×10^4 cells per well. Next, 500 μl of CM were added to the surface of Matrigel for additional 6-h incubation. The formed tubes for each well were then observed under the microscope. Then, the intracellular ROS scavenging ability of scaffolds was measured. In brief, a total of 2×10^4 per well HUVECs were plated into the lower chamber of 24-well plate and incubated at 37 °C overnight. Subsequently, cells in the positive group were incubated with H_2O_2 (100 μM) and the experimental groups were supplemented with H_2O_2 (100 μM) as well as with matched MSC or scaffolds on the upper chamber for 24 h. Then, HUVECs in each group were cultured with 10 μM of DCFH-DA probe for 20 min, followed by washing with PBS for three times. Finally, the cellular ROS levels were determined using a fluorescence microscope. The number of migrated cells, formed tubes, as well as ROS fluorescent intensity were all quantified from three randomly selected fields per well by image processing, with the analyst blinded to the group identity.

2.7. Hemolysis assay

A hemolysis assay was conducted to evaluate the hemolytic effect of the G/P scaffolds. Fresh blood (1 ml) was collected from a healthy female rat into a sodium citrate tube and centrifuged at 4000 rpm for 15 min. The anticoagulated plasma was discarded, and the resulting red blood cell (RBC) pellets were washed with ice-cold PBS (24 ml) to acquire a 4 % RBC suspension. Subsequently, the G/P scaffolds, immersed in 0.5 ml of PBS, were incubated with 0.5 ml of RBC suspension. The positive control was prepared by adding 0.5 ml of double deionized water (ddH_2O) into 0.5 ml of RBC suspension, and 0.5 ml of RBC suspension was mixed with 0.5 ml of PBS as negative control. Following a 3-h incubation at 37 °C, all samples were centrifuged at 4000 rpm for 5 min. The absorbance of the hemoglobin (HGB) in the supernatant was then measured at 570 nm to calculate the hemolysis ratio.

2.8. In vivo endometrial regeneration assay

All animal experimental procedures were performed in a sterile environment. First, each female Sprague-Dawley rat was administrated PMSG intraperitoneally at a dose of 200 U/kg for 3 days prior to surgery. All rats were anesthetized and the skin of the abdomen was disinfected with iodine. Then, a 3-cm midline incision was cut and muscle layers were separated. After that, the peritoneum was cut to enter the abdominal cavity. Using an ophthalmic scissor, an incision of 3 mm was created longitudinally on each side of the uterine body. A curette was employed to meticulously scrape the endometrial lining until the noticeable hyperemia occurred and the uterine wall turned coarse. A total of 25 female rats with dual uterus injuries were randomly divided into five groups (n = 5 per group): (1) Sham; (2) IUA; (3) G/P; (4) MSC; and (5) MSC@G/P. Next, the matched MSCs or scaffolds were transferred using a sterile forceps into the bilateral uteruses of the rats based

on the above grouping. The Sham and IUA groups received equal amounts of saline injected into the uterine cavity. The uterine cut and abdominal cavity were stitched layer by layer postoperatively, and each rat was administered 100,000 IU of penicillin daily for 3 days.

After 7 days had passed following treatments, the rats were sacrificed and the uteri were harvested. The uterine tissues were sliced into sections with a 5-μm thickness. The thickness of endometrium and the numbers of newly formed glands were assessed by H&E staining analysis. Masson trichrome staining was used to evaluate the collagen deposition. The immunohistochemical staining TNF-α and Ki-67 was used to evaluate inflammation and proliferation. A dual immunofluorescent staining of CD31 and α-SMA was performed to determin neovascularization. Additionally, ESRα and LIF immunofluorescent staining were conducted to assess endometrial receptivity. Meanwhile, fresh blood samples were collected from the rats of Sham, IUA, and MSC@G/P groups as well as additional normal healthy rats for hematological and biochemical analyses.

Fertility tests were performed to assess the endometrial receptivity after the MSC@G/P scaffolds treatment. A vaginal smear approach was used to assess the estrus cycle of rats. After two estrous cycles of treatment, female rats from Sham, IUA, and MSC@G/P groups (n = 5 per group) and sexually mature male rats were housed together at a 1:1 ratio, with the presence of a vaginal plug in a female rat on the following morning was recorded as day 0.5 of gestation. At day 10 of gestation, the number of embryo implantations was recorded in each group. All animal experiments have been reviewed and approved by the Institutional Animal Care and Use Committee of Wenzhou Medical University (wydw2024-0467).

2.9. Statistical analysis

Data statistical analysis was performed using GraphPad Prism 8.0 software (GraphPad, USA). At least three replicates were conducted in each experiment. All data were normally distributed and presented as mean ± standard deviation (SD). For analyzing the difference between groups, a Student's unpaired *t*-test or one-way analysis-of-variance (ANOVA) was carried out. Statistical significance was defined as $^{*}P < 0.05$, $^{**}P < 0.01$, and $^{***}P < 0.001$. Graphs were all depicted by Origin 2018 software (OriginLab, USA).

3. Results and discussion

MSCs have received increasing attention as promising candidate for tissue regeneration, with cells usually derived from bone marrow, adipose tissue and other sources [28]. Among these MSCs, AT-MSC has unique advantages for it can be isolated most abundantly and grows in high proliferation rates in mature animals [28,29]. Typically, human AT-MSC was successfully acquired and expanded according to our previous study [27]. First, the immunophenotypes of MSC were evaluated by flow cytometric assay. Results confirmed highly positive expressions of CD73, CD90, and CD105 (>95 %) on MSC, while negative expression of CD34 and CD11b (<2 %) (Fig. S1a). Subsequently, the in-vitro adipogenic and osteogenic capacities of MSC were assessed. It was noticed that evident oil droplets and calcium granules were observed by Oil Res O and Alizarin Red S staining, respectively (Fig. S1b).

Then, the thermos-reversibility of PF-127 and G/P hydrogels in the present study were assessed. As shown in Fig. S2a, PF-127 is a reverse thermosensitive polymer that undergoes a solution-to-gel transition upon increasing the temperature. The most crucial parameter for reversible polymers is their phase transition temperature [30,31]. No gelation of PF-127 was observed at either room temperature or 37 °C when the concentration was lower than 15 % w/v. By contrast, 15 % w/v PF-127 can form a gel at 37 °C (Fig. S2b). At higher concentrations (≥20 %), the PF-127 was gelled at both room temperature and 37 °C [17]. Then, the mixed solution with 15 % w/v GelMA and different concentrations of PF-127 (0, 5 %, 7.5 %, 10 %, 12.5 %, 15 %) were prepared. Results found that the gelation only occurred when GelMA (15 % w/v) was mixed with 15 % w/v of PF-127 at 37 °C. Therefore, PF-127 at 15 % w/v was selected as an optimal formulation for the construction of the composite hydrogel.

GelMA hydrogel, characterized by its high biocompatibility, biodegradability, and low immunogenicity, has been widely used for cell delivery [32,33]. Notably, numerous arginine-glycine-aspartic acid sequences within GelMA grant it with bioactive property [34]. Herein, the G/P scaffold was created by a microfluidic 3D printing technique. A bioink mixture solution composed of GelMA (15 % w/v) and PF-127 (15 % w/v) was prepared. Microfibers were gradually formed through extrusion from a suitable printhead nozzle on the microfluidic 3D printer. A good synchronization was found between the printing speed and the microfluidic flow rates. Then 60 % UV exposure was used during the printing process to achieve the initial solidification of scaffold fibers (Fig. 2a). The G/P scaffolds were fabricated by layering partially solidified microfibers during the printing process. Then the scaffolds were subsequently irradiated with 100 % UV after printing and then transferred into a 37 °C incubator to reinforce the structures. As shown in Fig. S3, the fiber thickness could be modified by altering the microfluidic flow rates. Moreover, the microfluidic-assisted printing strategy allowed for precise control of scaffold shapes (Fig. 2a), providing a stable flexibility and adaptability for practical use. The SEM images revealed a porous structure of the G/P scaffolds after freeze drying, as shown in Fig. 2b.

We then compared the mechanical properties between GelMA and G/P hydrogels by using the compression test. It could be obtained from Fig. 3a that the G/P hydrogels exhibited a mechanical strain of 66 % before fracture, surpassing the 56 % strain observed in the pure GelMA hydrogels. To observe how the storage modulus (G′) and loss modulus (G″) vary with temperature, the rheological test on PF-127 and GelMA was performed. As shown in Fig. 3b, for PF-127, the initial G′ was inferior to G″ when the temperature was <30 °C, corresponding to the sol state. Then, G′ and G″ formed a cross-over and G′ increased sharply at 37 °C, signifying that the sol-gel transition occurred. This result further confirmed the excellent thermos-responsive ability of PF-127 [17,30]. By contrast, the G′ and G″ values of GelMA hydrogel (after photo-crosslinking) remained largely unchanged across various temperatures.

Then, the *in vitro* biocompatibility of G/P scaffolds on AT-MSC was confirmed through co-culturing the scaffolds prior to cell seeding. As illustrated in Fig. S4, MSCs grew well and were still alive when co-cultured with G/P scaffolds for 5 days. MSCs were then encapsulated into G/P scaffolds, and their viability and growth within the scaffolds were investigated. As shown in Fig. S5, MSCs were successfully loaded within the G/P composite scaffolds and were distributed uniformly, retaining their viability for 5 days. In summary, these results support our subsequent study on the biological functions of the MSC@G/P. Angiogenesis is an important step for supplying nutrients and removing metabolites during tissue regeneration, with endothelial cells playing key roles in this process [35,36]. Herein, the regenerative capacities of MSC@G/P were investigated *in vitro* through experiments assessing the proliferation, migration, and tube formation of HUVECs (Fig. 4a–c). Our findings indicated that MSC@G/P markedly increased the cell viability, migration, and vessel formation compared to the G/P scaffold and MSC alone groups. This implies that MSC within the G/P scaffolds remained alive and released factors that continuously stimulated HUVECs. Moreover, our results revealed that the encapsulated MSC could be well protected inside the G/P scaffolds, and the cell behaviors could be effectively regulated by extending their duration time. The cellular ROS depletion ability of MSC@G/P scaffolds was determined using DCFH-DA as the fluorescence probe. H_2O_2 stimulation successfully induced the ROS generation as evidenced by a high fluorescent signal. The ROS levels were significantly reduced with MSC and MSC@G/P incubation, confirming their effective ability in ROS scavenging (Fig. S6). Taken together, the aforementioned *in vitro* results indicated that the

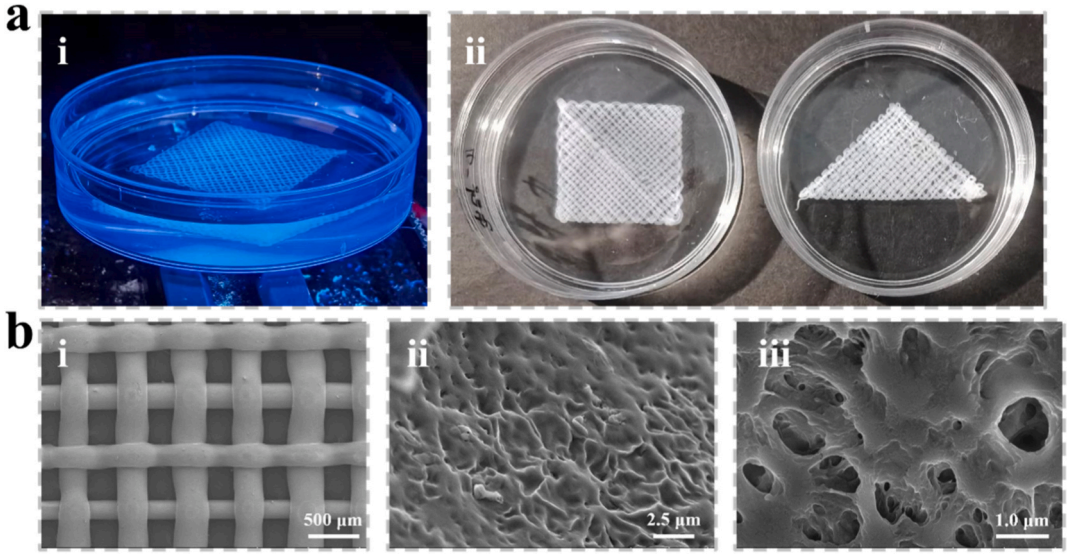

Fig. 2. Preparation of the G/P hydrogel scaffold. (a) The as-printed G/P scaffolds with different shapes (square and triangle). (b) SEM images of the G/P scaffolds.

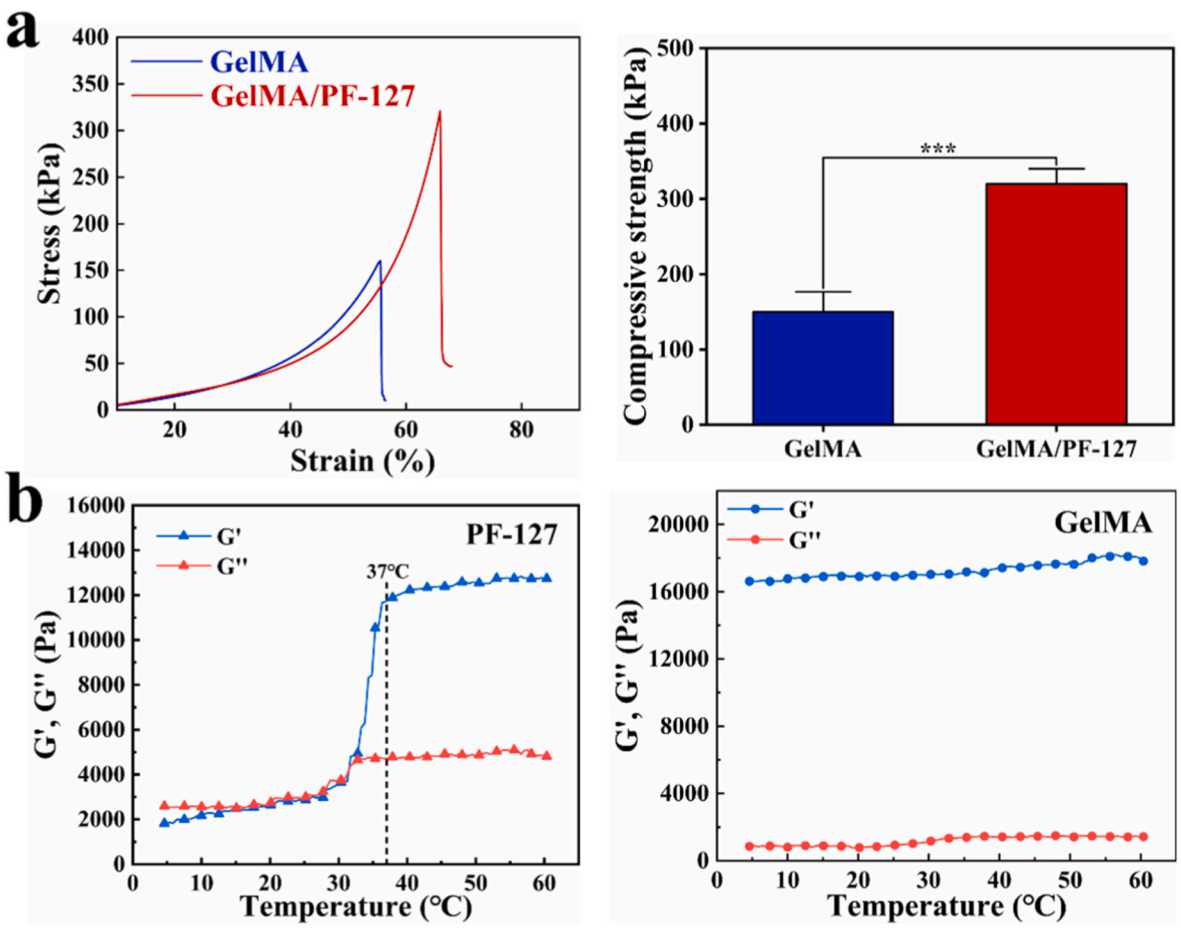

Fig. 3. Characterization of the hydrogel scaffolds. (a) Compression test results of different hydrogels. Data are means ± SD, n = 3, ***$p < 0.001$. (b) Temperature sweep of PF-127 and GelMA (after photo-crosslinking).

MSC@G/P could promote cell growth, migration, and angiogenesis, as well as inhibit oxidative stress.

We next developed an *in vivo* rat model of endometrial injury by mechanically scratching the uterine horn (Fig. S7), as previously described [26,37,38]. Biosafety assessment *in vivo* is crucial for evaluating the clinical feasibility of materials. To evaluate the hemocompatibility of the scaffold, a hemolysis assay was conducted before *in vivo* treatment studies. No color change was observed in the G/P scaffolds group when incubated with RBCs, suggesting that the hemolysis could be ignored (Fig. S8). Then, H&E staining kits were used to stain

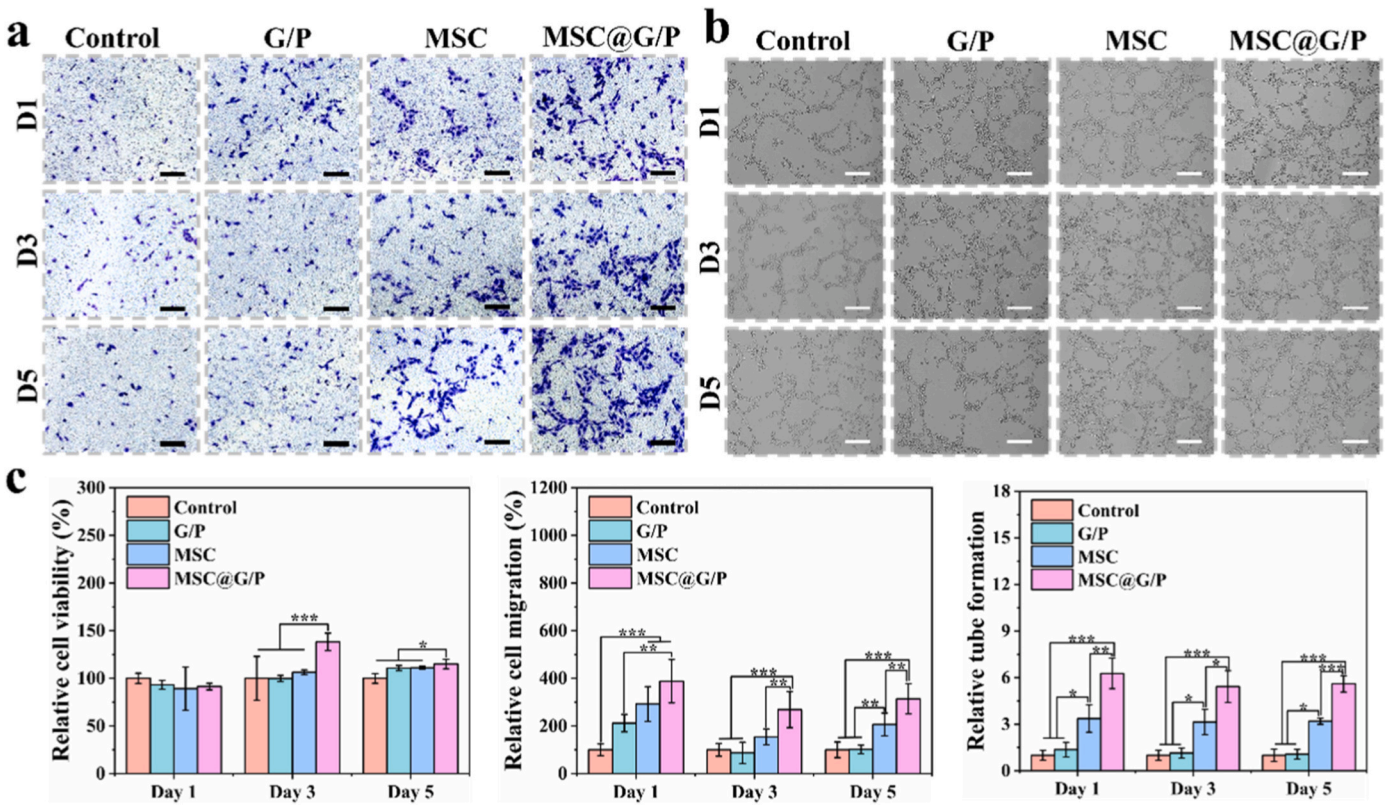

Fig. 4. The biological functions of different scaffolds *in vitro*. (a) Representative images of migrated HUVECs co-cultured with different scaffolds. Scale bar = 50 μm. (b) Representative images of HUVECs tube formation in different groups. Scale bar = 100 μm. (c) Quantification of cell viability, migration, and formed tube numbers of HUVEC with different treatments. Data are means ± SD, n = 3, $*p < 0.05$, $**p < 0.01$, $***p < 0.001$.

the major organs of each rat. Results showed no pathologic abnormalities occurred in these organs (Fig. S9). Furthermore, peripheral blood was collected from the rats of different groups (Sham, IUA, MSC@G/P) for a routine hematological analysis, as well as hepatic and renal function analyses. As we expected, the negligible effect of MSC@G/P scaffolds was supported by the normal levels of white blood cell (WBC), RBC, HGB, and platelet (PLT), as compared to normal rats (Fig. S10). Moreover, no significant alterations were detected in serum levels of alanine aminotransferase (ALT), aspartate aminotransferase (AST), albumin (ALB), alkaline phosphatase (ALP), total bilirubin (TBIL), hematuria nitrogen (UREA), and creatinine (CREA) of rats in different groups (Fig. S11). These results indicated that the MSC@G/P scaffolds had excellent biocompatibility *in vivo*.

A week after the model was established, endometrial injury was evaluated using appropriate histological examinations. In certain regions, the damaged uterine tissue showed notable edema and congestion of the uterine wall (Fig. S12). As displayed in Fig. 5a, the thickness of endometrium in the Sham operation group was measured 425.3 ± 14.5 μm, whereas it was markedly decreased into 273.8 ± 10.1 μm in the IUA model group and 268.8 ± 23.0 μm in the G/P group, respectively. The thickness was increased in the other treatment groups, with the MSC@G/P-treated rats reaching a peak thickness of 434.1 ± 33.6 μm, highlighting the strong regenerative capabilities of this composite hydrogel (Fig. 5c). The quantity of glands showed patterns similar trends across various treatment groups. In particular, rats treated with MSC@G/P had an average of 15.4 ± 2.8 glands, with this value comparable to the Sham operation group and roughly double that of the IUA group (Fig. 5c), confirming the effectiveness of the MSC@G/P scaffold in promoting endometrial regeneration.

The regenerative repertoire of the endometrium is seemingly overwhelmed by certain injuries especially related to medical procedures, resulting in endometrial fibrosis. In severe IUA cases, fibrotic lesions may span the uterine walls to form adhesions or synechiae, partially or even completely obstructing the uterine cavity [39]. The determination of the fibrotic states provides a valuable opportunity to evaluate the effects of endometrial regeneration [40]. Therefore, the Masson's trichrome staining was performed to assess collagen deposition in isolated uterine samples, showing that MSC notably reduced endometrium fibrosis and facilitated the growth of endometrial fibers (Fig. 5b and c). These findings also determined that the anti-fibrotic effects of MSC@G/P were significantly superior compared to that of MSC treatment alone, as evidenced by the percentage of collagen deposition in each group. This implies that our MSC@G/P hydrogel can efficiently alleviate inflammation and fibrosis by promoting the prolonged release of MSC, which in turn facilitates robust glandular growth in the rat endometrial damage.

TNF-α is a pro-inflammatory cytokine [41] and Ki-67 is a marker for cell proliferation [42], respectively. Given that the local inflammatory reactions and cell proliferation greatly influence the efficacy of endometrial regeneration [39], we performed immunohistochemical staining assays on TNF-α and Ki-67. As shown in Fig. 6, the pure G/P scaffold did not ameliorate the inflammation response caused by endometrial damage, while the treatments of MSC alone or MSC@G/P scaffold could significantly reduce inflammatory levels, as determined by the downregulation of TNF-α in the endometrial wounds. This is likely through the paracrine secretion of anti-inflammatory factors. Additionally, the Ki-67 staining results revealed that MSC@G/P achieved a significant proliferative effect, which was closely related to the strong paracrine function of MSC, potentially secreting growth factors.

Angiogenesis is crucial for supplying necessary oxygen and nutrients to healing lesions during tissue regeneration [35,36]. Hence, we next determined whether the MSC@G/P-mediated neovascularization observed *in vitro* was consistent with endometrial angiogenesis *in vivo*. For this purpose, endometrial tissue underwent dual staining for the

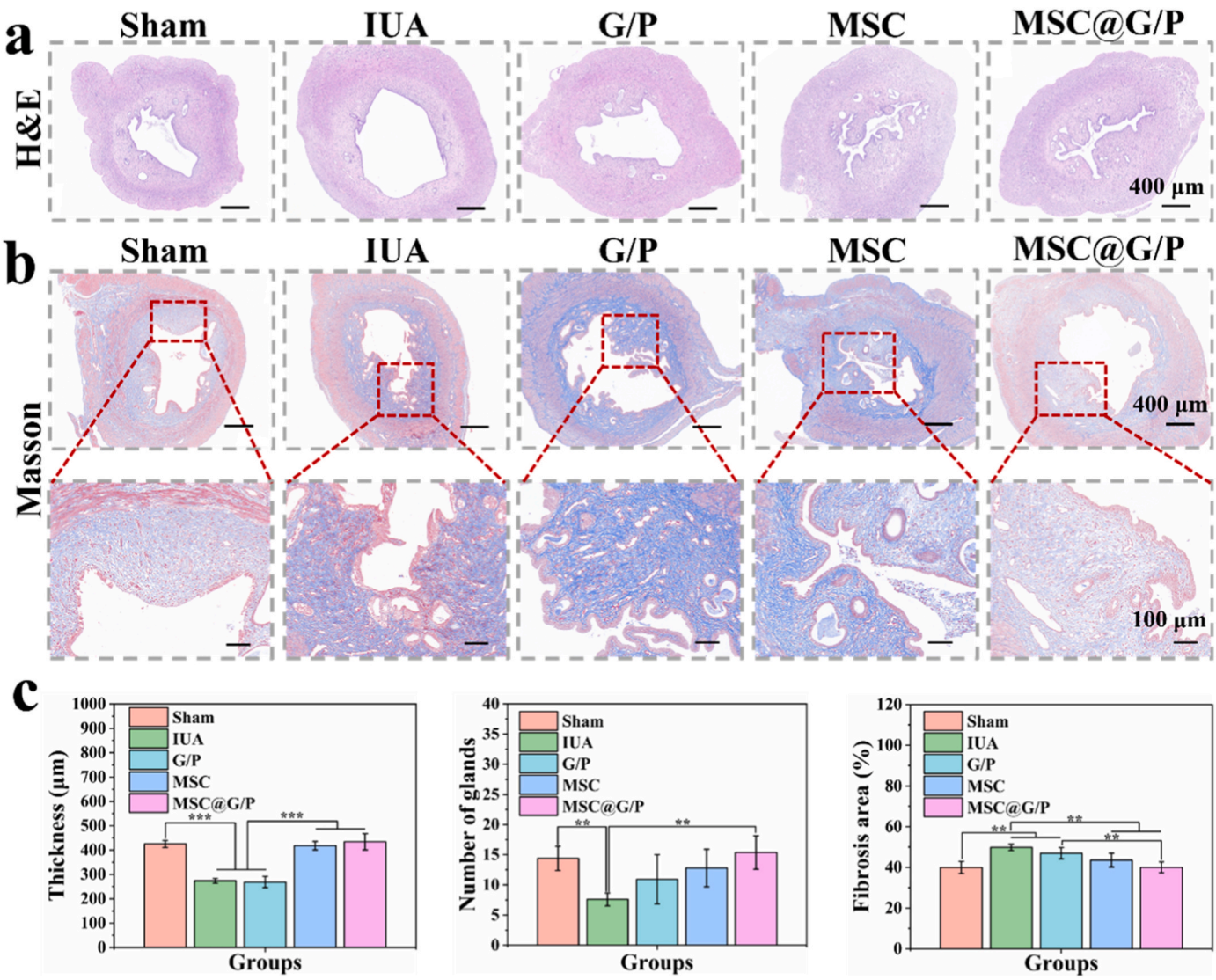

Fig. 5. Histological evaluation of alterations in uterine structure under different treatments. Uterine tissue sections are induced to (a) H&E staining (Scale bar = 400 μm) and (b) Masson staining (Scale bar = 400 μm & 100 μm). (c) Quantification of endometrial thicknesses (μm), gland numbers (uterine field of view), and fibrosis area (%) for each group. Data are means ± SD, n = 5, $^{**}p < 0.01$, $^{***}p < 0.001$.

endothelial cell marker CD31 and the vascular smooth muscle marker α-SMA. Results revealed that endometrial tissue samples from the MSC and MSC@G/P treatment groups exhibited a notable rise in CD31/α-SMA positive newly blood vessels compared to the IUA group, with the highest staining observed in the MSC@G/P scaffold treatment group. It is hypothesized that the MSC@G/P scaffold acts as a sustained-release system for MSC-derived angiogenic factors that likely promotes endothelial cell migration and tube formation, leading to the mature vasculature observed in our results. Endometrial receptivity is mediated by a variety of elements that orchestrate intrauterine modifications to support blastocyst implantation [43,44]. Two well-studied markers including LIF and ESRα were evaluated by immunofluorescent staining [45,46]. Consistent with the aforementioned findings, the MSC@G/P group exhibited the most intense fluorescence for LIF and the greatest positive rate for ESRα among all groups. These results may be attributed to MSC-secreted cytokines and indicates the role for MSC in re-establishing estrogen sensitivity. Collectively, the findings suggested that the MSC@G/P hydrogel scaffold could facilitate functional endometrial regeneration conducive to the fertility restoration.

To evaluate the impact of MSC@G/P scaffolds treatment on the endometrial receptivity recovery, the fertility of rats was assessed by recording the number of embryo implantations on gestational days 10 [47]. As shown in Fig. 7, embryo numbers were highest in the Sham group, as compared with that in both the IUA and MSC@G/P groups. Importantly, treatment of MSC@G/P within the uterine cavity improved the pregnancy rates apparently, while a significant disruption of fertility was occurred in rats of the IUA group. Therefore, our MSC@G/P scaffolds were able to promote functional endometrial regeneration conducive to the fertility restoration after curettage-induced endometrium damage.

4. Conclusion

In conclusion, we developed an MSC-loaded G/P composite hydrogel scaffold for promoting endometrial regeneration and dedicating to fertility restoration. The MSC@G/P hydrogel scaffold was suitable for effective delivery of MSC to facilitate tissue healing. Our research revealed that this hydrogel could enhance HUVEC growth, migration, and tube formation *in vitro*, and demonstrated a robust ability *in vivo* to stimulate neovascularization and suppress localized fibrosis during tissue repair. In summary, these findings suggest that the thermosensitive G/P scaffold loaded with MSC can facilitate the recovery of typical

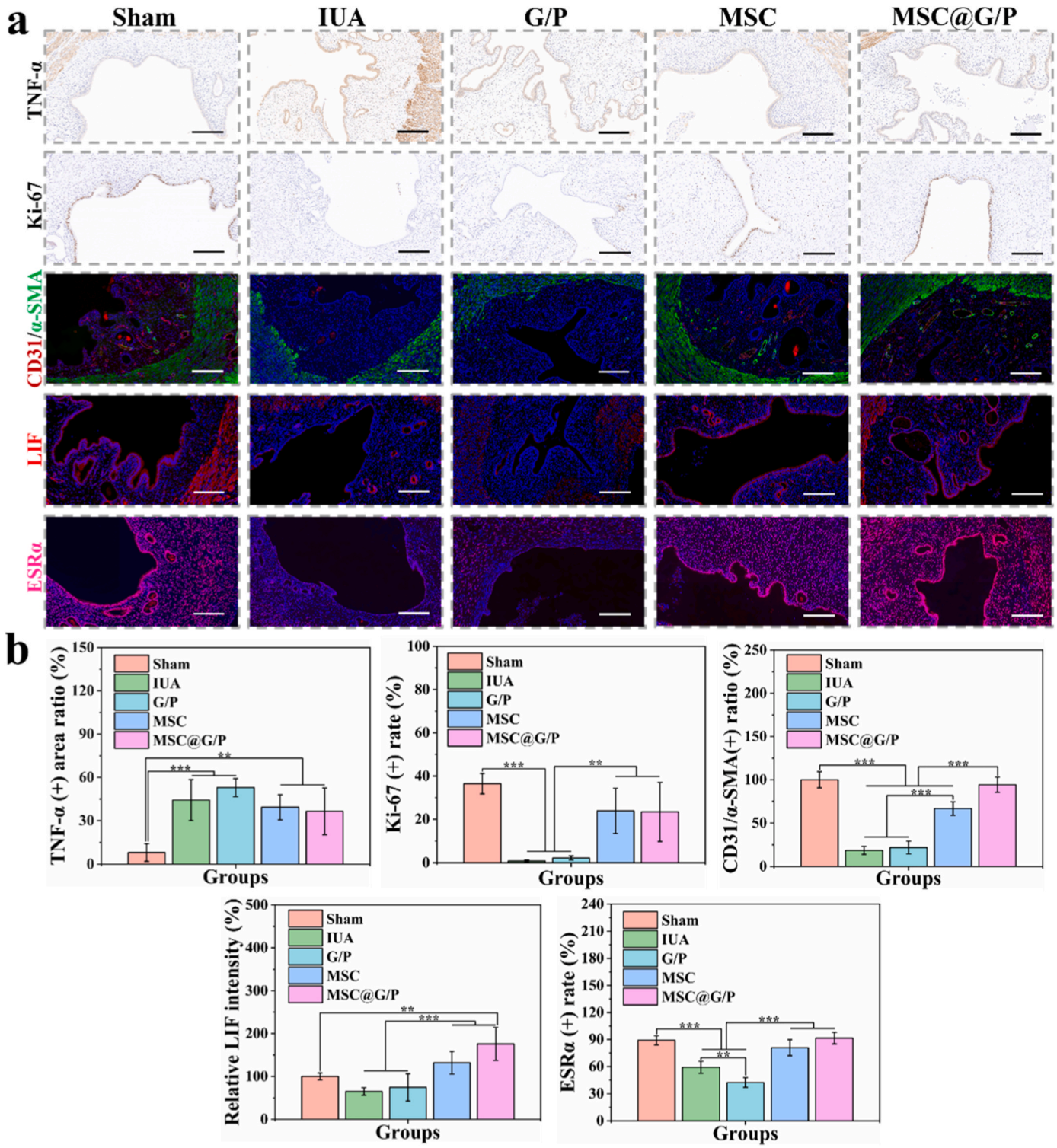

Fig. 6. *In vivo* endometrial regenerative capacity of different treatments. Immunohistochemical and immunofluorescent staining images of the uterine tissues from different groups. (a) TNF-α, Ki-67, CD31/α-SMA, LIF, and ESRα. Scale bar = 200 μm. (b) Quantification of immunohistochemical and immunofluorescent staining. Data are means ± SD, n = 5, $^{**}p < 0.01$, $^{***}p < 0.001$.

endometrial structure and function. Applying this composite hydrogel offers a potential strategy for clinically boosting endometrial regeneration.

CRediT authorship contribution statement

Yizuo Song: Writing – original draft, Formal analysis, Data curation. **Rong Ma:** Writing – review & editing, Methodology, Data curation. **Baozhu Yi:** Writing – review & editing, Methodology. **Qingfeng Zhou:** Writing – review & editing, Methodology. **Xiaosheng Li:** Writing – review & editing, Methodology. **Yujia Zhou:** Writing – review & editing, Methodology. **Ying Hua:** Writing – review & editing, Methodology. **Luoran Shang:** Writing – review & editing, Supervision, Conceptualization. **Xueqiong Zhu:** Writing – review & editing, Supervision,

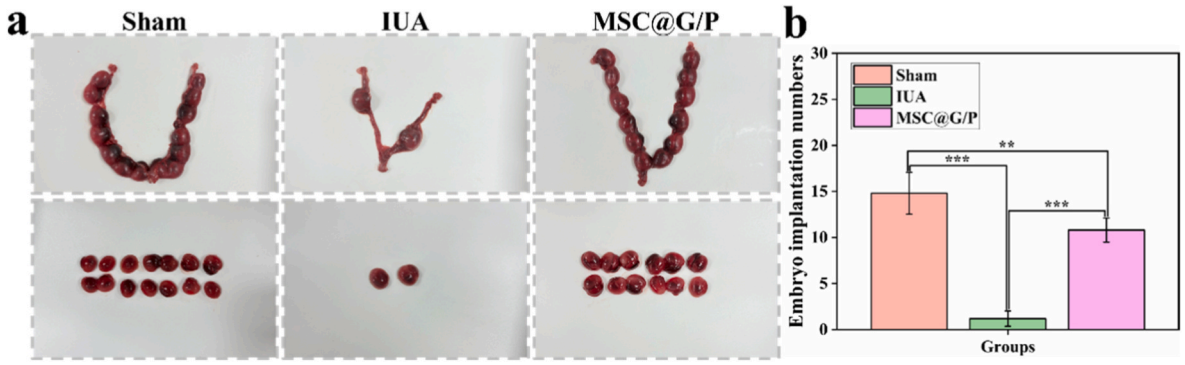

Fig. 7. The effect of MSC@G/P scaffolds treatment on fertility restoration. (a) Photographs of pregnant uterus and embryo sacs in different groups. (b) The number of embryo implantations in different groups. Data are means ± SD, n = 5, $^{**}p < 0.01$, $^{***}p < 0.001$.

Funding acquisition, Conceptualization.

Declaration of competing interest

The authors declare that they have no known competing financial interests or personal relationships that could have appeared to influence the work reported in this paper.

Acknowledgement

This study was supported by the grant from Wenzhou Major Science and Technology Innovation Project (ZY2022012).

Appendix A. Supplementary data

Supplementary data to this article can be found online at https://doi.org/10.1016/j.mtbio.2025.102742.

Data availability

Data will be made available on request.

References

[1] X. Santamaria, B. Roson, R. Perez-Moraga, N. Venkatesan, M. Pardo-Figuerez, J. Gonzalez-Fernandez, J. Llera-Oyola, E. Fernandez, I. Moreno, A. Salumets, H. Vankelecom, F. Vilella, C. Simon, Decoding the endometrial niche of Asherman's syndrome at single-cell resolution, Nat. Commun. 14 (1) (2023) 5890.
[2] R.M. Mortimer, A. Lanes, S.S. Srouji, I. Waldman, E. Ginsburg, Treatment of intrauterine adhesions and subsequent pregnancy outcomes in an in vitro fertilization population, Am. J. Obstet. Gynecol. (2024).
[3] B. Li, H. Chen, X. Lin, H. Duan, Multimodal learning system integrating electronic medical records and hysteroscopic images for reproductive outcome prediction and risk stratification of endometrial injury: a multicenter diagnostic study, Int. J. Surg. 110 (6) (2024) 3237–3248.
[4] A.B. Hooker, R.A. de Leeuw, J.W.R. Twisk, H.A.M. Brolmann, J.A.F. Huirne, Reproductive performance of women with and without intrauterine adhesions following recurrent dilatation and curettage for miscarriage: long-term follow-up of a randomized controlled trial, Hum. Reprod. 36 (1) (2021) 70–81.
[5] G. Chen, F. Wang, X. Zhang, Y. Shang, Y. Zhao, Living microecological hydrogels for wound healing, Sci. Adv. 9 (21) (2023) eadg3478.
[6] A. de Morree, T.A. Rando, Regulation of adult stem cell quiescence and its functions in the maintenance of tissue integrity, Nat. Rev. Mol. Cell Biol. 24 (5) (2023) 334–354.
[7] L. Fan, X. Zhang, L. Wang, Y. Song, K. Yi, X. Wang, H. Zhang, L. Li, Y. Zhao, Bio-inspired porous microneedles dwelled stem cells for diabetic wound treatment, Adv. Funct. Mater. 34 (28) (2024) 2316742.
[8] L. Wang, C. Yu, T. Chang, M. Zhang, S. Song, C. Xiong, P. Su, W. Xiang, In situ repair abilities of human umbilical cord-derived mesenchymal stem cells and autocrosslinked hyaluronic acid gel complex in rhesus monkeys with intrauterine adhesion, Sci. Adv. 6 (21) (2020) eaba6357.
[9] X. Yi, F. Liu, K. Gao, F. Chen, Y. Wang, H. Li, X. Wang, Y. Huang, H. Fu, W. Zhou, J. B. Fan, S. Wang, Y. Gao, Reconstructable uterus-derived materials for uterus recovery toward efficient live births, Adv. Mater. 34 (8) (2022) e2106510.
[10] S.R. Park, S.R. Kim, J.B. Im, C.H. Park, H.Y. Lee, I.S. Hong, 3D stem cell-laden artificial endometrium: successful endometrial regeneration and pregnancy, Biofabrication 13 (4) (2021).
[11] Y. Wang, J. Guo, X. Cao, Y. Zhao, Developing conductive hydrogels for biomedical applications, Smart Medicine 3 (1) (2024) e20230023.
[12] A. Rodriguez-Eguren, C. Bueno-Fernandez, M. Gomez-Alvarez, E. Frances-Herrero, A. Pellicer, J. Bellver, E. Seli, I. Cervello, Evolution of biotechnological advances and regenerative therapies for endometrial disorders: a systematic review, Hum. Reprod. Update 30 (5) (2024) 584–613.
[13] J. Wang, D. Huang, H. Chen, Y. Zhao, Biomimetic hepatic lobules from three-dimensional imprinted cell sheets, Sci. Bull. 69 (10) (2024) 1448–1457.
[14] W. Zhang, L. Cai, J. Gan, Y. Zhao, Photothermal responsive porous hollow microneedles as Chinese medicine versatile delivery system for wound healing, Smart Medicine 3 (3) (2024) e20240007.
[15] X. Lin, L. Cai, X. Cao, Y. Zhao, Stimuli-responsive silk fibroin for on-demand drug delivery, Smart Medicine 2 (2) (2023) e20220019.
[16] K.C. de Castro, J.C. Coco, E.M. Dos Santos, J.A. Ataide, R.M. Martinez, M.H.M. do Nascimento, J. Prata, P. da Fonte, P. Severino, P.G. Mazzola, A.R. Baby, E.B. Souto, D.R. de Araujo, A.M. Lopes, Pluronic(R) triblock copolymer-based nanoformulations for cancer therapy: a 10-year overview, J. Contr. Release 353 (2023) 802–822.
[17] M. Kiseleva, M.M. Omar, E. Boisselier, S.V. Selivanova, M.A. Fortin, A three-dimensional printable hydrogel formulation for the local delivery of therapeutic nanoparticles to cervical cancer, ACS Biomater. Sci. Eng. 8 (3) (2022) 1200–1214.
[18] D. Yan, W. Ouyang, J. Lin, Z. Liu, Smart coating by thermo-sensitive pluronic F-127 for enhanced corneal healing via delivery of biological macromolecule progranulin, Int. J. Biol. Macromol. 253 (Pt 8) (2023) 127586.
[19] Y. Zhu, B. Kong, R. Liu, Y. Zhao, Developing biomedical engineering technologies for reproductive medicine, Smart Medicine 1 (1) (2022) e20220006.
[20] C. Yang, Y. Yu, L. Shang, Y. Zhao, Flexible hemline-shaped microfibers for liquid transport, Nat. Chem. Eng. 1 (1) (2024) 87–96.
[21] Y. Liu, Q. Huang, J. Wang, F. Fu, J. Ren, Y. Zhao, Microfluidic generation of egg-derived protein microcarriers for 3D cell culture and drug delivery, Sci. Bull. 62 (18) (2017) 1283–1290.
[22] Y. Li, D. Yan, F. Fu, Y. Liu, B. Zhang, J. Wang, L. Shang, Z. Gu, Y. Zhao, Composite core-shell microparticles from microfluidics for synergistic drug delivery, Sci. China Mater. 60 (6) (2017) 543–553.
[23] H. Zhang, G. Chen, Y. Yu, J. Guo, Q. Tan, Y. Zhao, Microfluidic printing of slippery textiles for medical drainage around wounds, Adv. Sci. (Weinh.) 7 (16) (2020) 2000789.
[24] H. Wang, Z. Zhao, Y. Liu, C. Shao, F. Bian, Y. Zhao, Biomimetic enzyme cascade reaction system in microfluidic electrospray microcapsules, Sci. Adv. 4 (6) (2018) eaat2816.
[25] X. Wang, C. Yang, Y. Yu, Y. Zhao, In Situ 3D Bioprinting Living Photosynthetic Scaffolds for Autotrophic Wound Healing, 2022, Research (Wash D C), 2022 9794745.
[26] S. Lu, X. Wang, W. Li, Y. Zu, J. Xiao, Injectable 3D-Printed porous scaffolds for adipose stem cell delivery and endometrial regeneration, Adv. Funct. Mater. 33 (34) (2023) 2303368.
[27] Y. Song, X. Shou, B. Sheng, J. Mei, K. Shi, L. Shang, X. Zhu, Cell membranes from tumor-tropic MSCs screened by a microfluidic chip for drug nanoparticles encapsulation and cancer targeted therapy, Adv. Healthcare Mater. 12 (17) (2023) e2202904.
[28] M. Kamal, D. Kassem, K.H. Haider, Sources and therapeutic strategies of mesenchymal stem cells in regenerative medicine, in: K.H. Haider (Ed.), Handbook of Stem Cell Therapy, Springer Singapore, Singapore, 2022, pp. 1–28.
[29] J.Q. Yin, J. Zhu, J.A. Ankrum, Manufacturing of primed mesenchymal stromal cells for therapy, Nat. Biomed. Eng. 3 (2) (2019) 90–104.
[30] B. Shriky, A. Kelly, M. Isreb, M. Babenko, N. Mahmoudi, S. Rogers, O. Shebanova, T. Snow, T. Gough, Pluronic F127 thermosensitive injectable smart hydrogels for controlled drug delivery system development, J. Colloid Interface Sci. 565 (2020) 119–130.
[31] X. Wu, T. Liu, H. Li, Y. He, G. Yang, W. Zhu, T. Chen, Sol-gel transition effect based on konjac glucomannan thermosensitive hydrogel for photo-assisted uranium extraction, Sci. Bull. (2024).

[32] A.G. Kurian, R.K. Singh, K.D. Patel, J.H. Lee, H.W. Kim, Multifunctional GelMA platforms with nanomaterials for advanced tissue therapeutics, Bioact. Mater. 8 (2022) 267–295.
[33] R. Huang, X. Zhang, W. Li, L. Shang, H. Wang, Y. Zhao, Suction cups-inspired adhesive patch with tailorable patterns for versatile wound healing, Adv. Sci. (Weinh.) 8 (17) (2021) e2100201.
[34] K. Yue, G. Trujillo-de Santiago, M.M. Alvarez, A. Tamayol, N. Annabi, A. Khademhosseini, Synthesis, properties, and biomedical applications of gelatin methacryloyl (GelMA) hydrogels, Biomaterials 73 (2015) 254–271.
[35] G. Eelen, L. Treps, X. Li, P. Carmeliet, Basic and therapeutic aspects of angiogenesis updated, Circ. Res. 127 (2) (2020) 310–329.
[36] E.E. Crouch, A. Bhaduri, M.G. Andrews, A. Cebrian-Silla, L.N. Diafos, J.O. Birrueta, K. Wedderburn-Pugh, E.J. Valenzuela, N.K. Bennett, U.C. Eze, C. Sandoval-Espinosa, J. Chen, C. Mora, J.M. Ross, C.E. Howard, S. Gonzalez-Granero, J. F. Lozano, M. Vento, M. Haeussler, M.F. Paredes, K. Nakamura, J.M. Garcia-Verdugo, A. Alvarez-Buylla, A.R. Kriegstein, E.J. Huang, Ensembles of endothelial and mural cells promote angiogenesis in prenatal human brain, Cell 185 (20) (2022) 3753–3769 e18.
[37] Y. Cai, F. Wu, Y. Yu, Y. Liu, C. Shao, H. Gu, M. Li, Y. Zhao, Porous scaffolds from droplet microfluidics for prevention of intrauterine adhesion, Acta Biomater. 84 (2019) 222–230.
[38] L. Xin, C. Wei, X. Tong, Y. Dai, D. Huang, J. Chen, L. Ma, S. Zhang, In situ delivery of apoptotic bodies derived from mesenchymal stem cells via a hyaluronic acid hydrogel: a therapy for intrauterine adhesions, Bioact. Mater. 12 (2022) 107–119.
[39] C.J. Ang, T.D. Skokan, K.L. McKinley, Mechanisms of regeneration and fibrosis in the endometrium, Annu. Rev. Cell Dev. Biol. 39 (2023) 197–221.
[40] H. Sun, J. Dong, Z. Fu, X. Lu, X. Chen, H. Lei, X. Xiao, S. Chen, J. Lu, D. Su, Y. Xiong, Z. Fang, J. Mao, L. Chen, X. Wang, TSG6-Exo@CS/GP attenuates endometrium Fibrosis by inhibiting macrophage activation in a Murine IUA model, Adv. Mater. 36 (21) (2024) e2308921.
[41] D. Siegmund, H. Wajant, TNF and TNF receptors as therapeutic targets for rheumatic diseases and beyond, Nat. Rev. Rheumatol. 19 (9) (2023) 576–591.
[42] R. Sales Gil, P. Vagnarelli, Ki-67: more hidden behind a 'Classic Proliferation Marker', Trends Biochem. Sci. 43 (10) (2018) 747–748.
[43] R.J. Paulson, Introduction: endometrial receptivity: evaluation, induction and inhibition, Fertil. Steril. 111 (4) (2019) 609–610.
[44] A.D.S. Pathare, M. Loid, M. Saare, S.B. Gidlof, M. Zamani Esteki, G. Acharya, M. Peters, A. Salumets, Endometrial receptivity in women of advanced age: an underrated factor in infertility, Hum. Reprod. Update 29 (6) (2023) 773–793.
[45] M.A. Brennan, P. Layrolle, D.J. Mooney, Biomaterials functionalized with MSC secreted extracellular vesicles and soluble factors for tissue regeneration, Adv. Funct. Mater. 30 (37) (2020).
[46] L. Craciunas, I. Gallos, J. Chu, T. Bourne, S. Quenby, J.J. Brosens, A. Coomarasamy, Conventional and modern markers of endometrial receptivity: a systematic review and meta-analysis, Hum. Reprod. Update 25 (2) (2019) 202–223.
[47] X. Zheng, R. Huang, L. Yin, M. Yao, J. Chu, F. Yang, Y. Dong, M. Zhao, T. Ma, Injectable antioxidant hyaluronan/chitosan hydrogel as a platelet-rich plasma and stem cell carrier to promote endometrial regeneration and fertility restoration, Acta Biomater. 195 (2025) 201–215.